Controllable and tunable topological multiport beam splitter in an extended Su-Schrieffer-Heeger array

Ming-jie Liao, Mei-Song Wei, Yi-Qing Wang, Jingping Xu,* and Yaping Yang†
MOE Key Laboratory of Advanced Micro-Structured Materials, School of Physics Science and Engineering, Tongji University, Shanghai 200092, China

(Received 4 June 2024; accepted 23 August 2024; published 6 September 2024)

We demonstrate a controllable and tunable topological beam splitter with a multiport based on the one-dimensional extended Su-Schrieffer-Heeger model, which supports the topological interface by introducing the nearest-neighbor (NN) coupling defect at the central site. The quantum state initially prepared at the interface can be transmitted with high fidelity to multiple output ports with equal or unequal probability on both sides of the model by modulating the NN coupling between the sites in the time domain. We show that the output port can be added by increasing the number of sublattices a. Especially, by setting the on-site potential energy, we can easily control the direction of the quantum state transfer process and ensure that this state is only transmitted to the multiple output ports on the left or multiple output ports on the right, which realizes the function of topological switching. Benefiting from the topological protection of the edge states, the quantum states can be transmitted with high fidelity even if there is the NN coupling disorder. Our work realizes a robust and multifunctional topological beam splitter.

DOI: 10.1103/PhysRevA.110.032406

I. INTRODUCTION

Reliable and controllable quantum state transfer (QST) is one of the important components of quantum networks, and the efficiency of QST between different nodes directly affects the accuracy of the quantum communication process [1–5]. However, the process of QST is inevitably affected by system defects and environmental disturbances, which leads to the decoherence effect [6,7]. In order to improve the fidelity of QST, a variety of effective schemes have been proposed, such as quantum error correction [8–10], dynamical decoupling [11–13], and dark mode assistance [14–16]. In recent years, high-fidelity and robust QST processes have been demonstrated in topological insulators that benefit from protected topological boundary states [17–24].

In recent years, topological insulators have been widely studied in condensed-matter physics because of their conductive boundary states and insulating bulk states [25–30]. Different from traditional insulators, topological insulators have nonequivalence energy bands in momentum space [31–36]. The topological boundary state is immune to the local disturbance and disorder of the environment [37–39], so it can be used to transmit information efficiently and unidirectionally, making it an excellent QST platform [40–45]. For example, the Su-Schrieffer-Heeger (SSH) model, as the simplest one-dimensional topological insulator, has been successfully used for robust and high-fidelity quantum state transfer processes. Mei *et al.* constructed an extended SSH model by plugging superconducting qubits into a tunable array, and they demonstrated that single-qubit and two-qubit entangled states can achieve robust transmission over long distances [21]. Moreover, the quantum state transfer process can be accelerated by controlling the strength of the nearest-neighbor hopping and introducing next-neighbor coupling [22,23]. Obviously, the above studies focus on the transfer of quantum states from one site to another, and the system has only one input port and one output port. In Ref. [24], the interface can be introduced by splicing two Rice-Mele models, and then the initial state prepared on the interface (as an input port) can be transmitted to two ports on both sides with equal probability. Reference [46] shows a planar tunable transport scheme that can increase the number of output ports by increasing the number of SSH chains, but there is always only one input port. However, complex quantum networks may require more input and output ports than just a single input port. Therefore, in order to realize diversified information distribution and transmission in quantum networks, it is necessary to construct a topologically protected channel that includes multiple input ports and output ports.

In this paper, by splicing the extended SSH models, as displayed in Fig. 1, we propose a multiport input and output scheme. We can realize the transfer of the quantum state initially prepared at the interface to multiple ports with equal or unequal probability by controlling the nearest-neighbor coupling at the interface. Specifically, when the interface site is coupled equally to the left site and the right site, the energy will be evenly transmitted to both ends, but when the coupling is unequal, a variety of distributions can be displayed. In addition to the Hermitian case, we also consider the non-Hermitian case, where gain and loss are added at the lattice site. In general, the nonuniform loss at the sites can be equivalent to the gain-loss system. We find that the quantum states prepared at the interface only transfer to the left multiple output ports or the right output ports by controlling the gain-loss on the

*Contact author: xx_jj_pp@tongji.edu.cn
†Contact author: yang_yaping@tongji.edu.cn

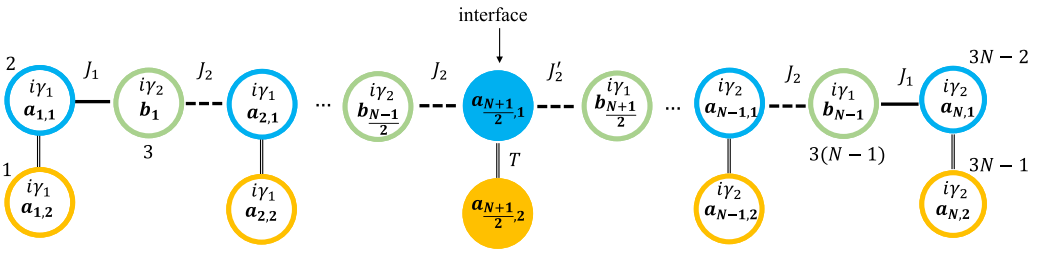

FIG. 1. The diagrammatic sketch of the extended SSH model with modulated nearest-neighbor hopping. Each unit cell has three sites and the size of this array is $L = 3N - 1$ (N is the number of unit cells and is odd). The NN hopping $J_{1,2}$ and the on-site gain and loss $\gamma_{1,2}$ except interface sites we considered.

lattice. This can be understood as the quantum state being preferentially transferred to the side of the effective gain. Therefore, it can be constructed as bidirectional topological switches with multiple input and output ports. In addition, we find that topological beam splitters with more ports can be constructed by increasing the number of sublattices a. When considering the disorder in the NN coupling, we find that the QST channel can still achieve high-fidelity transmission with slight interference.

The paper is organized as follows: In Sec. II, we introduce an extended SSH model that enables multiport input and output. On the one hand, the extended SSH model can realize topological beam splitters with equal or unequal probability, and on the other hand, bidirectional topological switches can be constructed by adjusting the on-site potential. The QST channel is immune to disorder. In Sec. III, we show how to construct more input and output ports by adding sublattices a. Finally, we give a brief conclusion in Sec. IV.

II. TOPOLOGICAL BEAM SPLITTER BY EDGE PUMPING IN A SPLICING EXTENDED SSH MODEL

A. Model and Hamiltonian

To establish a controlled topological beam splitter, we consider a splicing extended SSH model as shown in Fig. 1. This lattice consist of three sublattice sites, $a_{n,1}$, $a_{n,2}$, and b_n, with $n = 1, 2, \ldots, N$, in each unit cell and the total site number is $L = 3N - 1$. Here, the lattice size N is set as an odd number, so that the extended SSH model has a topological interface at site $a_{N+1/2}$. This system can be governed by the Hamiltonian [47–49], as seen in Eq. (1).

Here, $J_1 = J_0[1 + \cos(\frac{\pi t}{t^*})]$ and $J_2 = J_0[1 - \cos(\frac{\pi t}{t^*})]$ are the modulated coupling strengths of nearest-neighbor hopping while $\gamma_{1,2}$ is the strength of on-site gain and loss. t^* is the total transfer time. T denotes the coupling between sites $a_{n,1}$ and $a_{n,2}$ for each unit cell of the SSH array, respectively. At the topological interface, J_2 and J_2' denote hopping between interface sites and nearest-neighbor sites. When $\gamma_{1,2} = 0$, this system returns to the Hermitian:

$$
\begin{aligned}
H = & \sum_{n=1}^{N/2-1} [-i\gamma_1 a_{n,1}^\dagger a_{n,1} - i\gamma_1 a_{n,2}^\dagger a_{n,2} - i\gamma_2 b_n^\dagger b_n] \\
& + \sum_{n=\frac{N+1}{2}+1}^{N} [-i\gamma_2 a_{n,1}^\dagger a_{n,1} - i\gamma_2 a_{n,2}^\dagger a_{n,2} - i\gamma_1 b_n^\dagger b_n] \\
& + \sum_{n=1}^{N/2-1} [T a_{n,1}^\dagger a_{n,2} + J_1 a_{n,1}^\dagger b_n + J_2 a_{n+1,1}^\dagger b_n + \text{H.c.}] \\
& + \sum_{n=\frac{N+1}{2}+1}^{N} [T a_{n,1}^\dagger a_{n,2} + J_2 a_{n,1}^\dagger b_n + J_1 a_{n+1,1}^\dagger b_n + \text{H.c.}] \\
& + \sum_{n=\frac{N+1}{2}} [T a_{n,1}^\dagger a_{n,2} + i\gamma_1 b_n^\dagger b_n + J_2' a_{n,1}^\dagger b_n + J_1 a_{n+1,1}^\dagger b_n \\
& + \text{H.c.}]. \qquad (1)
\end{aligned}
$$

To explore the topological character of the array, we now consider a finite-sized lattice array without gain or loss with $J_2 = J_2'$. Figure 2(a) displays the energy spectrum of the system with size $N = 5$; it clearly shows that the topological edge states (marked red) are located at the bulk gaps. We plot the eigenstate distribution of the upper red gap state. Obviously, the gap state is mainly distributed in a-type sites at the interface when $J_1 > J_2$ ($t/t^* \in [0, 0.5] \cup [1.5, 2]$), but when $J_1 < J_2$ ($t/t^* \in [0.5, 1.5]$), it is mainly distributed at the two ends of the array, as displayed in Fig. 2(b). Particularly, by diagonalizing Eq. (1) under the open boundary condition, this state can be described as

$$
\begin{aligned}
|\Psi\rangle = & |1, 1, 0, \eta, \eta, 0, \eta^2, \eta^2, 0, \ldots, \eta^{\frac{N+1}{2}}, \eta^{\frac{N+1}{2}}, \\
& 0, \ldots, 0, \eta^2, \eta^2, 0, \eta, \eta, 0, 1, 1\rangle. \qquad (2)
\end{aligned}
$$

where $\eta = -J_1/J_2$ manifests the probability amplitude hinge on NN hopping J_1 and J_2. Equation (2) is consistent with the behaviors shown in Fig. 2(b).

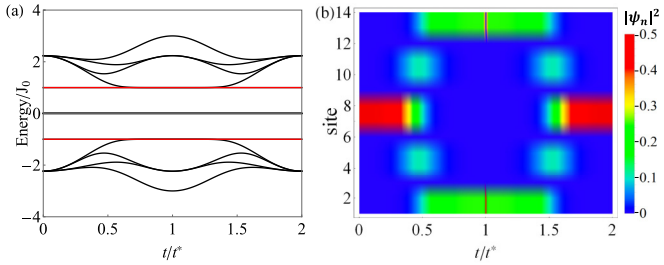

FIG. 2. (a) The energy spectrum of this array with $\gamma_{1,2} = 0$, in which the two red lines denote topological edge states. (b) The distribution of the edge states [located in the upper band gap of panel (a)] as a function of t/t^*. The system parameters are set to $T = 1$ and $L = 3N - 1 = 14$.

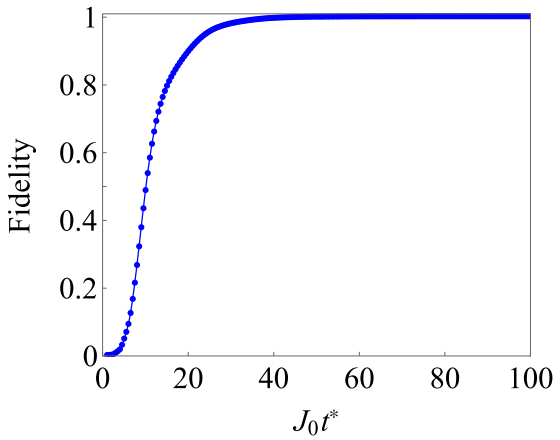

FIG. 3. Fidelity F as a function of total transfer time t^*. We set the initial state $\Psi(0) = 1/\sqrt{2}|0, 0, 0, 0, \ldots, 1, 1, \ldots, 0, 0, 0, 0\rangle$ and other parameters are the same as those Fig. 2.

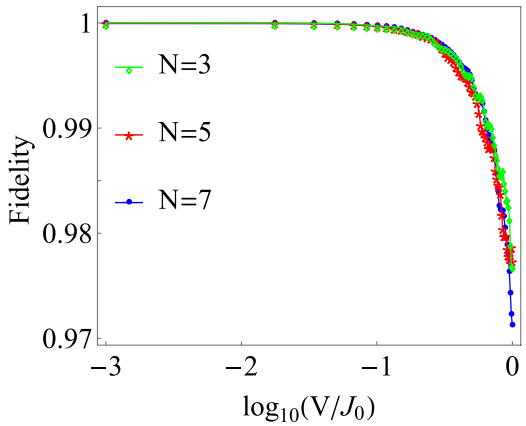

FIG. 5. Fidelity F as a function of NN disorder with different sizes of N. Green squares, red asterisks, and blue dots indicate system sizes $N = 3, 5$, and 7, respectively. Here, we consider $J_0t^* = 150$ and another parameter set as $T = 1$.

Based on Fig. 2, if we consider the a-type sites at the interface as two input ports, and the $a_{1,1}$, $a_{1,2}$, $a_{N,1}$, and $a_{N,2}$ sites as the four output ports, then this lattice array can be regarded as a topological beam splitter and realize quantum state transfer from multiple ports to multiple ports. On the other hand, the QST process is protected by the gap and immune to some disorders. In order to illustrate the reliability of the beam splitter on the topological QST process, we can use transfer fidelity for evaluation and the fidelity is defined as $F = |\langle\Psi_f|\Psi(t^*)\rangle|^2$. Here, $|\Psi_f\rangle$ represents an ideal final state we need, in which $\Psi_f = 1/\sqrt{4}|1, 1, 0, 0, \ldots, 0, 0, 1, 1\rangle$, and $|\Psi(t^*)\rangle$ is the evolved final state in the real space, which can be obtained by solving the Schrödinger equation $i\frac{\partial\Psi}{\partial t} = H|\Psi\rangle$. Figure 3 displays transfer fidelity versus total evolution time t^*. It is clearly shown that $F \to 1$ when $J_0t^* > 40$ and the topological edge transfer is under adiabatic evolution. Figure 4 plots the distribution of edge states in the gap with different transfer times. When $J_0t^* = 10$, energy does not transfer well from the interface sites to the two ends, as displayed in Fig. 4(a). However, when we added J_0t^* to 60, as seen in Fig. 4(b), energy can be transferred adiabatically from the two interface ports to the four edge ports with equal probability. So, this multiport beam splitter that depends on the topological edge channel is successful on the one-dimensional (1D) array.

Benefiting from the development of quantum optics and wave optics, a series of excellent experimental platforms have emerged. Our QST scheme is based on a one-dimensional extended SSH model, which can be easily implemented in superconducting systems (qubit arrays and resonator arrays) [50–52] and waveguide arrays [53–55]. In addition to this, the use of ultracold atoms in optical lattices is also widely used to study various topological topics [56–58]. For example, for the multiport topological beam splitter, we can use a series of waveguide arrays. The NN hopping and on-site potential energy are modulated by adjusting the distance between waveguides and the refractive index of individual waveguides. However, in practice, the coupling parameters cannot be completely accurate. Therefore, it is necessary to evaluate the robustness of the topological beam splitter. Here, the disorder adding to system can be governed by

$$J_1 \to J_1 + \delta V, \quad J_2 \to J_2 + \delta V, \quad T \to T + \delta V, \tag{3}$$

where V is the strength of disorder and δ is a random number within the range $[-0.5, 0.5]$. For each δV, we choose 100 samples and average them. In order to guarantee the adiabatic evolution of the QST process, we choose the total transfer time of $J_0t^* = 150$.

Figure 5 shows the relationship between average fidelity and disorder during quantum state transfer for different system sizes N ($N = 3$, 5, and 7). Clearly, the proposed topological beam splitter can maintain sufficiently high fidelity during the quantum state transfer when the strength of the NN hopping disorder is $-3 < \log_{10}(V/J_0) < -1$. Therefore, the multiport beam splitter is robust to slight disorder during the QST process.

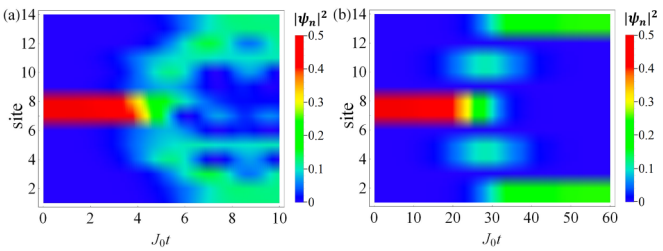

FIG. 4. Evolution of the upper gap state with different total transfer time. (a) $J_0t^* = 10$. (b) $J_0t^* = 60$. We take $T = 1, L = 3N - 1 = 14$, and $\gamma_1 = \gamma_2 = 0$, and the initial state is the same as that in Fig. 3.

B. Multiport beam splitter with unequal probabilities

We have demonstrated a topological beam splitter that can be transmitted to both ends with equal probability, because the interface site has the same coupling weight as the left and right sites, and that perfectly implements multiport-to-multiport transmission in this 1D model. Next, we investigate a multiport beam splitter with unequal probabilities, i.e., $J_2 \neq J_2'$. When $J_1 : J_2 = 2 : 1$, we plot the energy spectrum in Fig. 6(a1), and it has two gap states similar to Fig. 2(a).

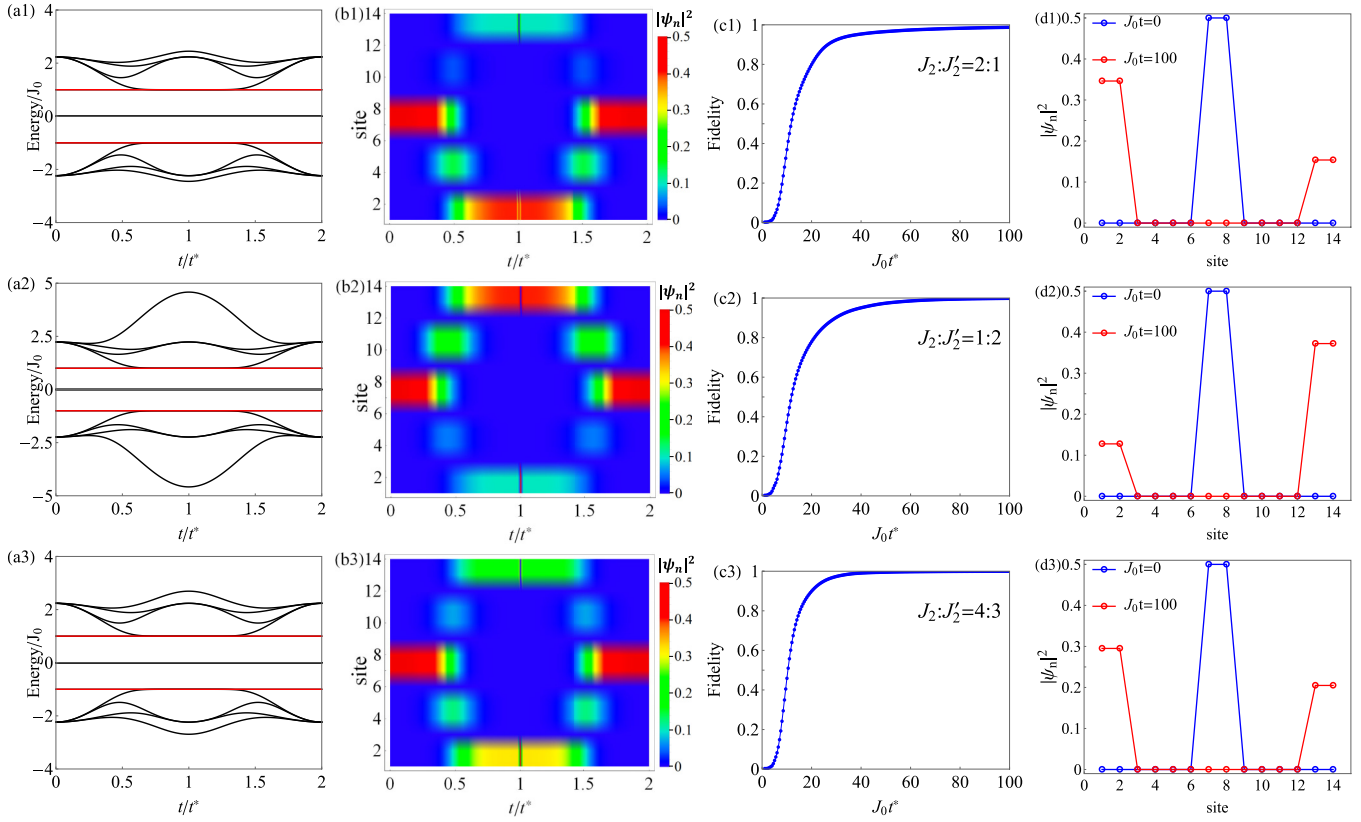

FIG. 6. Energy spectrum, distribution of the gap state, and fidelity. The energy spectra of the extended SSH model are shown in panels (a1)–(a3), and the red lines are the edge states with (a1) $J_1 : J_2 = 2 : 1$, (a2) $J_1 : J_2 = 1 : 2$, and (a3) $J_1 : J_2 = 4 : 3$. The distribution of the edge states versus t/t^* corresponds to panels (b1)–(b3), respectively. We prepare the initial state at the interface and it can be transferred to four output ports with unequal probability, and the fidelity versus total evolved time t^* is shown in panels (c1)–(c3). Panels (d1)–(d3) show the quantum state transfer process when $J_0t = 0$ or $J_0t = 100$.

The probability distribution of the upper edge state is shown in Fig. 6(b1). We can see that the energy mainly occupies two resonators at the interface when the normalized time is $t/t^* \in [0, 0.5] \cup [1.5, 2]$, while it is distributed in the four resonators at the edge within $t/t^* \in [0.5, 1.5]$. In particular, the adiabatic QST process is realized within the transfer total time $J_0t^* > 100$ and the high fidelity $F \approx 1$, as seen in Fig. 6(c1). In the process of quantum state evolution, we show that the initial state is prepared with equal probability at two ports on the interface. This state is transferred from the interface sites to both ends, and the probability distribution of the four end ports is $2.3 : 2.3 : 1 : 1$ when $J_0t = 100$, as seen in Fig. 6(d1). In this way, we construct an unequal probability topological beam splitter with two-port input and four-port output.

Similarly, by modulating the NN coupling at the interface, we can realize that more QST channels benefit from the nonuniform distribution of the edge states. We also display the QST process within $J_1 : J_2 = 1 : 2$ and $J_1 : J_2 = 4 : 3$. Although the energy spectra of these two cases are different, the two edge states always exist with the change of normalization time t/t^*, as can be seen from Figs. 6(a2) and 6(a3). Distribution of the eigenstate as a function of t/t^* is shown in Figs. 6(b2) and 6(b3). The probability transfers from two sites at the interface to both ends of the array with unequal probabilities, and the QST process has high fidelity when $J_0t^* > 70$ and $J_0t^* > 40$, respectively. The probability distribution of the final state about the four end ports is $1 : 1 : 2.9 : 2.9$ with $J_1 : J_2 = 1 : 2$ and $5 : 5 : 7 : 7$ with $J_1 : J_2 = 4 : 3$ of the four out ports. Namely, it is clearly shown that multiport and tunable beam splitters can be implemented.

In order to test the robustness of this probability-adjustable topological beam splitter, we plot the average fidelity versus the disorder, as seen in Fig. 6. Similarly, to satisfy adiabatic evolution in QST, we take $J_0t^* = 120$. Figure 7 shows the fidelity average based on 100 samples. For different couplings at the interface, we find that, when $\log_{10}(V/J_0) < -0.7$, the transmission fidelity is $F \to 1$. Similar to a multiport topological beam splitter with equal probability, the quantum state can still be transferred to the target ports with high fidelity when a small perturbation is applied to the system.

C. Multiport beam splitter with topological switch

To further understand this multibeam splitter, we consider the effects of adding gain-loss to the system. In this case, the eigenvalues are complex numbers. The real part and the imaginary part of the energy spectrum are shown in Figs. 8(a) and 8(b), respectively. Clearly, the real part $\mathrm{Re}(E)$ of the edge state always has the symmetric eigenvalues $\mathrm{Re}(-E)$ located in the bulk gaps, and the imaginary parts of two edge states are always equal.

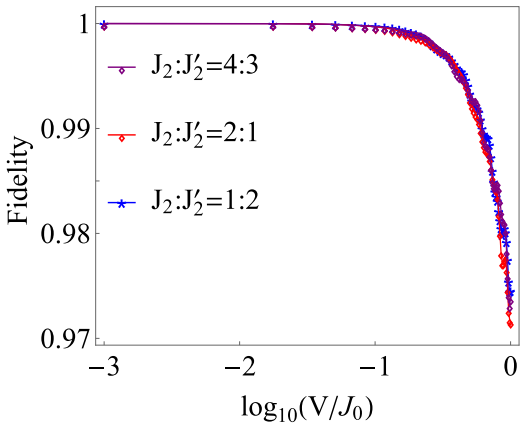

FIG. 7. Fidelity as a function of disorder V with unequal coupling at interface sites. The size of the array is $N = 5$ and the total transfer time is $J_0 t^* = 120$.

Figure 9 reflects the effect of unbalanced loss on the distribution of the edge state. It is widely known that unbalanced loss is equivalent to the gain-loss system. Figure 9 displays the upper edge state versus normalized time t/t^*. When we consider $\gamma_1 = 0.2$ and $\gamma_2 = 0.4$, it can be seen from Fig. 9(a) that this state is mainly distributed in the central sites corresponding to $J_1 > J_2$ and located at the left ports corresponding to $J_1 < J_2$. However, when $\gamma_1 = 0.4$ and $\gamma_2 = 0.2$, as shown in Fig. 9(b), the probability distribution for this edge state is reversed from Fig. 9(a). Therefore, we can conclude that the QST process is transmitted to the left two ports with $\gamma_1 < \gamma_2$, because $-i\gamma_1 a^\dagger_{1,i} a_{1,i}$ is equivalent to an effective gain compared to $-i\gamma_2 a^\dagger_{N,i} a_{N,i}$ ($i = 1$ and 2), and it is transmitted to the right two ports with $\gamma_1 > \gamma_2$. $\gamma_1/\gamma_2 = 1$ is a critical value, and the direction of the topological beam splitter can be selected by adding effective on-site gain and loss.

Here, in order to further understand the effect of virtual on-site potential energy added to sites on quantum state transfer, we simulate the system evolution process corresponding to different values of $\gamma_{1,2}$. First, for $\gamma_1 < \gamma_2$, fidelity and topological excitation transfer are exhibited in Figs. 10(a1)–10(d1). Herein, $|L\rangle$ and $|R\rangle$ represent the ideal left and right edge states, denoted as $|L\rangle = 1/\sqrt{2}|1, 1, \ldots, 0, 0, \ldots, 0, 0\rangle$ and $|R\rangle = 1/\sqrt{2}|0, 0, \ldots, 0, 0, \ldots, 1, 1\rangle$, respectively. Comparing Figs. 10(a1) and 10(b1), the quantum state initially prepared at the interface is efficiently transmitted to the left

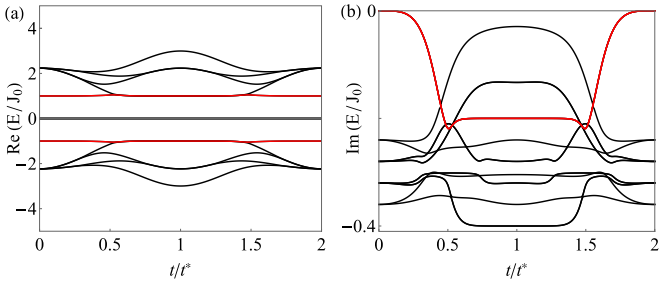

FIG. 8. Energy spectrum. (a) The real part and (b) the imaginary part of the energy spectrum with $\gamma_1 = 0.4$ and $\gamma_2 = 0.2$. Other parameters are the same as those in Fig. 2.

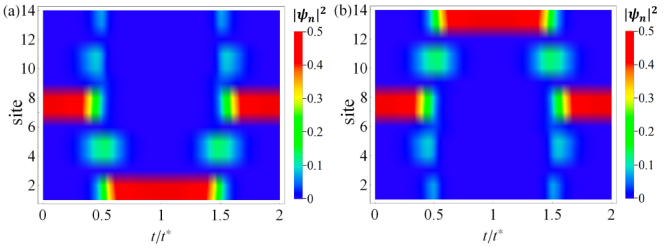

FIG. 9. The distribution of the upper gap state as a function of t/t^* with (a) $\gamma_1 = 0.2$ and $\gamma_2 = 0.4$ and (b) $\gamma_1 = 0.4$ and $\gamma_2 = 0.2$.

ports but cannot be transferred to the right output ports, and when total evolution time $J_0 t^* > 60$, the fidelity of the quantum state transferred to the left side is $F \to 1$. For $J_0 t^* = 80$, the dynamic evolution of the system with time is shown in Fig. 10(c1), which displays the QST from central multiple input ports to left multiple output ports. To make the state distribution in the QST process more clear, we plot the probability distribution at $J_0 t = 0$ and $J_0 t = 80$ in Fig. 10(d1). Moreover, for $\gamma_1 > \gamma_2$, we also plot the fidelity and topological excitation transfer in Figs. 10(a2)–10(d2), which are in sharp contrast to the results of $\gamma_1 < \gamma_2$. In addition, we also analyzed the case when $\gamma_1 = \gamma_2$. In this case, the density distribution of the system gap states is similar to that in the Hermitian case. When $J_1 > J_2$, the density is distributed at the interface, while when $J_1 < J_2$, the density is mainly distributed at the sublattice a on both sides of the array. Therefore, when the system is at a uniform loss, the QST process is similar to the Hermitian case.

Next, we continue to discuss the quantum state transfer of the system when γ_1 and γ_2 are positive and negative, respectively. For $\gamma_1 = -0.2$ and $\gamma_2 = 0.4$, the quantum state can be transmitted to the left end of the array with extremely high fidelity when $J_0 t^* > 20$. According to Eq. (1), when $\gamma_1 < 0$ and $\gamma_2 > 0$, $-i\gamma_1 a^\dagger_{1,i} a_{1,i}$ correspond to gain sites and $-i\gamma_2 a^\dagger_{N,i} a_{N,i}$ ($i = 1$ and 2) correspond to loss sites. Therefore, when we prepare the initial state at the interface, it passes towards the left end of the array, as shown in Figs. 10(a3)–10(d3). But for $\gamma_1 > 0$ and $\gamma_2 < 0$, as displayed in Figs. 10(a4)–10(d4), it is shown that the quantum state is only transmitted to the right side of the array. To sum up, in our quantum state transfer scheme, when the initial state is prepared at the interface, the quantum state is biased towards the gain-sublattice transfer, which can realize the function of topological switching, consistent with our discussion above.

So far, we have implemented a multiport topological beam splitter with equal or unequal probability distribution based on the extended SSH model and controlled the direction of the QST process through on-site gain or loss so as to realize the function of topology switching.

III. EXTENDED MULTIPORT BEAM SPLITTER BY ADDING SUBLATTICES A

In the above, we have shown the controlled QST process in which quantum states can be transferred from the interface to multiple output ports in different forms. Here, we can increase the input and output ports by adding the sublattices

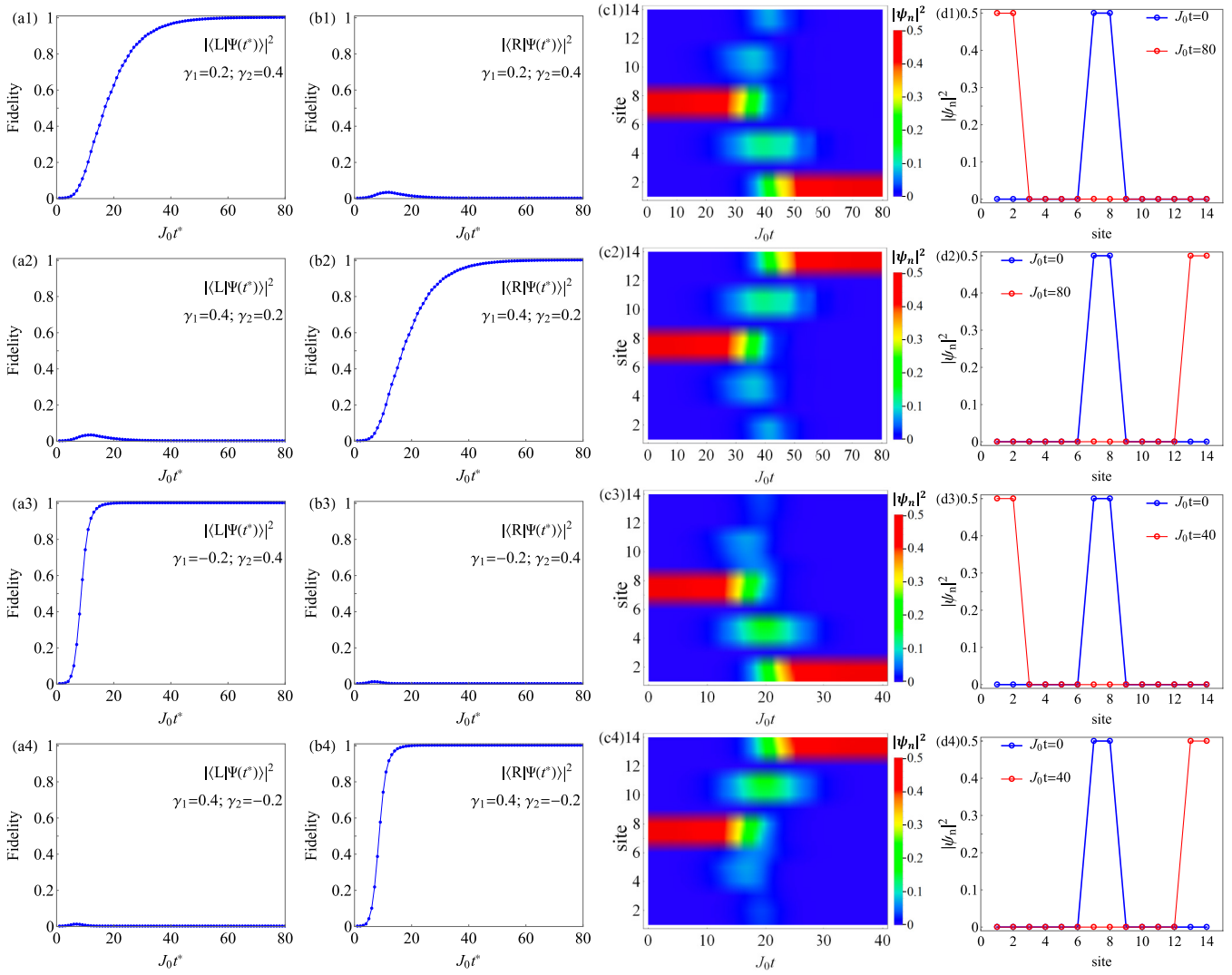

FIG. 10. Fidelity and topological excitation transfer. Evolution of the initial state is $|\Phi(0)\rangle = 1/\sqrt{2}|0, 0, \ldots, 1, 1, \ldots, 0, 0\rangle$, and it is shown that the initial state is evenly distributed in the middle two sites. (a1)–(a4) Fidelity F for quantum state transfer to the left edge versus transfer total time t^*. (b1)–(b4) Fidelity F for quantum state transfer to the right edge versus transfer total time t^*. The evolution of the system with $J_0t^* = 80$ for panels (c1) and (c2) and $J_0t^* = 40$ for panels (c3) and (c4). Quantum state distribution with $J_0t = 0$ or $J_0t = 80$ for panels (d1) and (d2) and $J_0t = 0$ or $J_0t = 40$ for panels (d3) and (d4). The parameters are $\gamma_1 = 0.2$ and $\gamma_2 = 0.4$ for panels (a1)–(d1), $\gamma_1 = 0.4$ and $\gamma_2 = 0.2$ for panels (a2)–(d2), $\gamma_1 = -0.2$ and $\gamma_2 = 0.4$ for panels (a3)–(d3), and $\gamma_1 = 0.4$ and $\gamma_2 = -0.2$ for panels (a4)–(d4).

a. Figure 11 shows a schematic of a model that implements more input and output ports. Now, we consider sublattices a that contain three sites, and we can control quantum state transmission from the interface to both ends of the array by adjusting the hopping between lattice sites.

Figure 12(a) displays the probability amplitude distribution of an edge state with normalized time t/t^*. Clearly, it is shown that, if we change the hopping J_1 from 0 to 2 and the hopping J_2 from 2 to 0, the quantum states initially prepared at the interface will evolve to both sides of the array. This also reveals the potential application of this model to construct a topological beam splitter. Subsequently, we investigate the fidelity of this QST process. We think about the initial state being $|\Phi_0\rangle = |0, 0, 0, \ldots, \frac{1}{2}, \frac{\sqrt{2}}{2}, \frac{1}{2}, \ldots, 0, 0, 0\rangle$, and the ideal final state of evolution is $|\Phi\rangle = |\frac{\sqrt{2}}{4}, \frac{1}{2}, \frac{\sqrt{2}}{4}, \ldots, 0, 0, 0, \ldots, \frac{\sqrt{2}}{4}, \frac{1}{2}, \frac{\sqrt{2}}{4}\rangle$. The fidelity as a function of total transfer time t^* is seen in Fig. 12(b), where it is displayed that the quantum state can be transferred to the output port in high quality when $J_0t^* > 80$. On the other hand, it also shows that when the evolution time is long enough, the system follows adiabatic topological transmission. For $J_0t^* = 100$, the process of topological state transfer is shown in Fig. 12(c). During this evolution, the probability amplitude of the input ports is $a_{3,1} : a_{3,2} : a_{3,3} = 1 : 2 : 1$ when $t = 0$ and the amplitudes of the output ports are $a_{1,1} : a_{1,2} : a_{1,3} = 1 : 2 : 1$ and $a_{5,1} : a_{5,2} : a_{5,3} = 1 : 2 : 1$ when $J_0t = 100$, as exhibited in Fig. 12(d). The simulation shows that the edge state in this extended SSH system can be used as a topology channel to realize multiple output ports.

Similarly, to analyze the robustness to disorder of the quantum state transmission process with multiple input ports, as shown in Fig. 13, we plot the fidelity of the QST from the interface to both ends as a function of the disorder strength.

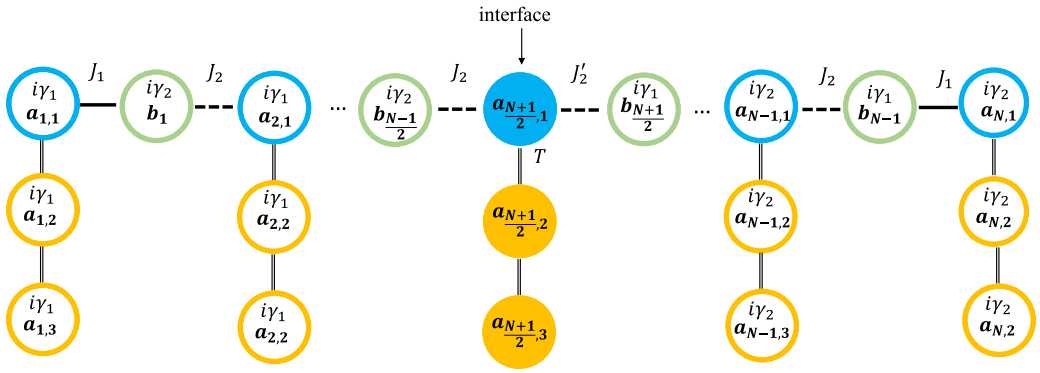

FIG. 11. Schematic diagram of the extended SSH resonator array to realize more ports. Here, each unit cell contains four resonators. For this model, the number of output ports is controlled by controlling the number of sublattices a.

The numerical results show that, when the disorder strength is $\log_{10}(V/J_0) < -0.3$, the quantum state can be transmitted perfectly, and the fidelity is $F \to 1$. Therefore, it is feasible to implement the operation of multiple input ports by increasing the sublattice a, which is robust to slight perturbations. This facilitates the construction of complex quantum networks.

IV. CONCLUSIONS

In conclusion, we have revealed a scalable and robust topological multiport beam splitter based on the extended SSH model. On the one hand, the output ports with equal or unequal probabilities can be realized by adjusting the coupling between the two sides of the sites at the interface. On the other hand, we can control the number of ports of the topological beam splitter by increasing the number of sublattices a. Benefiting from the topological protection of edge states, we find that the system is robust to nearest-neighbor coupling disorder during the quantum state transfer process. Moreover, we can flexibly control the direction of the output port by adjusting the ratio of on-site potential energy. When $\gamma_1 < \gamma_2$, topology transmission is biased to the left ports, while when $\gamma_1 > \gamma_2$, topology transmission is biased to the right ports. When $\gamma_1 = \gamma_2$ and the interface state is initially excited, the quantum state is transferred to both the left and right ends. Our research provides a reference for multiport transmission based on a one-dimensional structure.

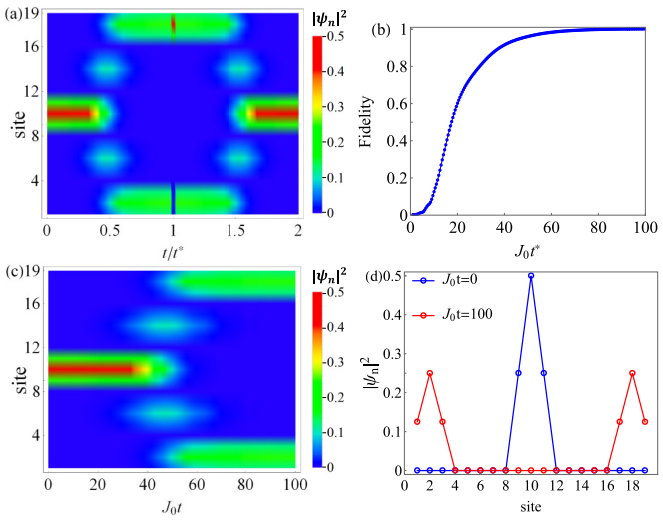

FIG. 12. (a) The probability amplitude of a gap mode versus t/t^*. (b) Fidelity of the quantum state initially prepared at the interface sites transferred to $a_{n,1}$, $a_{n,2}$, and $a_{n,3}$ ($n = 1$ and 5). (c) The process of quantum state transfer with the total evolution time $J_0t^* = 100$. (d) The probability distribution of the evolution state at different times. The size of the system $L = 4N - 1 = 19$, $T = 1$, and $\gamma_1 = \gamma_2 = 0$.

ACKNOWLEDGMENTS

This work is supported by the National Natural Science Foundation of China (Grants No. 12274326 and No. 12174288) and the National Key R & D Program of China (Grant No. 2021YFA1400602).

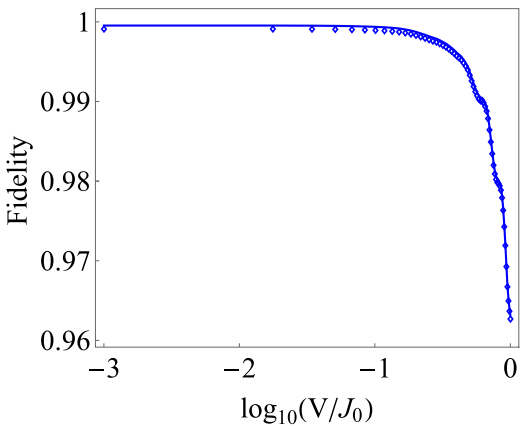

FIG. 13. The fidelity F of the quantum state transfer process against the NN coupling disorder. The size of the array is $N = 5$ and the total transfer time is $J_0t^* = 100$. The other parameters are the same as those in Fig. 12.

[1] B. Yurke and J. S. Denker, Quantum network theory, Phys. Rev. A **29**, 1419 (1984).

[2] J. I. Cirac, P. Zoller, H. J. Kimble, and H. Mabuchi, Quantum state transfer and entanglement distribution among distant nodes in a quantum network, Phys. Rev. Lett. **78**, 3221 (1997).

[3] A. Galindo and M. A. Martín-Delgado, Information and computation: Classical and quantum aspects, Rev. Mod. Phys. **74**, 347 (2002).

[4] C. Simon, Towards a global quantum network, Nat. Photon. **11**, 678 (2017).

[5] P. Kurpiers, P. Magnard, and T. Walter, Deterministic quantum state transfer and remote entanglement using microwave photons, Nature (London) **558**, 264 (2018).

[6] S. A. Gurvitz and D. Mozyrsky, Quantum mechanical approach to decoherence and relaxation generated by fluctuating environment, Phys. Rev. B **77**, 075325 (2008).

[7] J. Paavola and S. Maniscalco, Decoherence control in different environments, Phys. Rev. A **82**, 012114 (2010).

[8] A. Kay, Quantum error correction for state transfer in noisy spin chains, Phys. Rev. A **93**, 042320 (2016).

[9] M. H. Michael, M. Silveri, R. T. Brierley, V. V. Albert, J. Salmilehto, L. Jiang, and S. M. Girvin, New class of quantum error-correcting codes for a bosonic mode, Phys. Rev. X **6**, 031006 (2016).

[10] B. Vermersch, P. O. Guimond, H. Pichler, and P. Zoller, Quantum state transfer via noisy photonic and phononic waveguides, Phys. Rev. Lett. **118**, 133601 (2017).

[11] L. Viola, E. Knill, and S. Lloyd, Dynamical decoupling of open quantum systems, Phys. Rev. Lett. **82**, 2417 (1999).

[12] J. Du, X. Rong, and N. Zhao, Preserving electron spin coherence in solids by optimal dynamical decoupling, Nature (London) **461**, 1265 (2009).

[13] G. de Lange, Z. H. Wang, D. Riste, V. V. Dobrovitski, and R. Hanson, Universal dynamical decoupling of a single solid-state spin from a spin bath, Science **330**, 60 (2010).

[14] Y. L. Zhou, Y. M. Wang, L. M. Liang, and C. Z. Li, Quantum state transfer between distant nodes of a quantum network via adiabatic passage, Phys. Rev. A **79**, 044304 (2009).

[15] Y.-D. Wang and A. A. Clerk, Using dark modes for high-fidelity optomechanical quantum state transfer, New J. Phys. **14**, 105010 (2012).

[16] C. S. Zhao, Z. Yang, D. W. Wang, Y. T. Yan, C. Li, Z. H. Wang, and L. Zhou, Quantum networks assisted by dark modes in optomagnonic systems, Phys. Rev. A **108**, 043703 (2023).

[17] N. Y. Yao, C. R. Laumann, A. V. Gorshkov, H. Weimer, L. Jiang, J. I. Cirac, P. Zoller, and M. D. Lukin, Topologically protected quantum state transfer in a chiral spin liquid, Nat. Commun. **4**, 1585 (2013).

[18] S. Tan, R. W. Bomantara, and J. Gong, High-fidelity and long-distance entangled-state transfer with Floquet topological edge modes, Phys. Rev. A **102**, 022608 (2020).

[19] Y. L. Chang, J. J. Xue, Y. X. Han, X. L. Wang, and H. R. Li, Robust quantum state transfer with topologically protected nodes, Phys. Rev. A **108**, 062409 (2023).

[20] J. N. Zhang, J. X. Han, J. L. Wu, J. Song, and Y. Y. Jiang, Robust beam splitter with fast quantum state transfer through a topological interface, Front. Phys. **18**, 51303 (2023).

[21] F. Mei, G. Chen, L. Tian, S. L. Zhu, and S. T. Jia, Robust quantum state transfer via topological edge states in superconducting qubit chains, Phys. Rev. A **98**, 012331 (2018).

[22] F. M. D'Angelis, F. A. Pinheiro, D. Guéry-Odelin, S. Longhi, and F. Impens, Fast and robust quantum state transfer in a topological Su-Schrieffer-Heeger chain with next-to-nearest-neighbor interactions, Phys. Rev. Res. **2**, 033475 (2020).

[23] N. E. Palaiodimopoulos, I. Brouzos, F. K. Diakonos, and G. Theocharis, Fast and robust quantum state transfer via a topological chain, Phys. Rev. A **103**, 052409 (2021).

[24] L. Qi, Y. Xing, X. D. Zhao, S. T. Liu, S. Zhang, S. Hu, and H. F. Wang, Topological beam splitter via defect-induced edge channel in the Rice-Mele model, Phys. Rev. B **103**, 085129 (2021).

[25] M. Z. Hasan and C. L. Kane, Colloquium: Topological insulators, Rev. Mod. Phys. **82**, 3045 (2010).

[26] X. L. Qi and S. C. Zhang, Topological insulators and superconductors, Rev. Mod. Phys. **83**, 1057 (2011).

[27] S. Q. Shen, *Topological Insulators [M]* (Springer, Berlin, 2012).

[28] T. Ozawa, H. M. Price, A. Amo, N. Goldman, M. Hafezi, L. Lu, M. C. Rechtsman, D. Schuster, J. Simon, O. Zilberberg, and I. Carusotto, Topological photonics, Rev. Mod. Phys. **91**, 015006 (2019).

[29] J. E. Moore, The birth of topological insulators [J], Nature (London) **464**, 194 (2010).

[30] C. K. Chiu, H. Yao, and S. Ryu, Classification of topological insulators and superconductors in the presence of reflection symmetry, Phys. Rev. B **88**, 075142 (2013).

[31] J. E. Moore and L. Balents, Topological invariants of time-reversal-invariant band structures, Phys. Rev. B **75**, 121306(R) (2007).

[32] R. Yu, X. L. Qi, A. Bernevig, Z. Fang, and X. Dai, Equivalent expression of Z_2 topological invariant for band insulators using the non-Abelian Berry connection, Phys. Rev. B **84**, 075119 (2011).

[33] L. J. Lang, X. M. Cai, and S. Chen, Edge states and topological phases in one-dimensional optical superlattices, Phys. Rev. Lett. **108**, 220401 (2012).

[34] A. Bansil, H. Lin, and T. Das, Colloquium: Topological band theory, Rev. Mod. Phys. **88**, 021004 (2016).

[35] N. R. Cooper, J. Dalibard, and I. B. Spielman, Topological bands for ultracold atoms, Rev. Mod. Phys. **91**, 015005 (2019).

[36] B. Y. Xie, H. X. Wang, X. J. Zhang, P. Zhan, J. H. Jiang, M. H. Lu, and Y. F. Chen, Higher-order band topology, Nat. Rev. Phys. **3**, 520 (2021).

[37] Q. S. Wu, L. Du, and V. E. Sacksteder, Robust topological insulator conduction under strong boundary disorder, Phys. Rev. B **88**, 045429 (2013).

[38] C. He, X. Ni, H. Ge, X. C. Sun, Y. B. Chen, M. H. Lu, X. P. Liu, and Y. F. Chen, Acoustic topological insulator and robust one-way sound transport, Nat. Phys. **12**, 1124 (2016).

[39] L. Chen, Z. F. Wang, and F. Liu, Robustness of two-dimensional topological insulator states in bilayer bismuth against strain and electrical field, Phys. Rev. B **87**, 235420 (2013).

[40] W. P. Su, J. R. Schrieffer, and A. J. Heeger, Soliton excitations in polyacetylene, Phys. Rev. B **22**, 2099 (1980).

[41] Y. E. Kraus, Y. Lahini, Z. Ringel, M. Verbin, and O. Zilberberg, Topological states and adiabatic pumping in quasicrystals, Phys. Rev. Lett. **109**, 106402 (2012).

[42] L. N. Zheng, L. Qi, L. Y. Cheng, H. F. Wang, and S. Zhang, Defect-induced controllable quantum state transfer via a topologically protected channel in a flux qubit chain, Phys. Rev. A **102**, 012606 (2020).

[43] M. S. Wei, M. J. Liao, Y. Q. Wang, Z. J. Lin, X. Z. Qiu, C. Wang, J. P. Xu, and Y. P. Yang, Quantum state transfer on square lattices with topology, Phys. Rev. A **108**, 062401 (2023).

[44] M. S. Wei, Y. Q. Wang, M. J. Liao, Z. J. Lin, C. Wang, J. P. Xu, and Y. P. Yang, Quantum state transfer on 1-dimensional and 2-dimensional topological Heisenberg spin models, Results Phys. **54**, 107026 (2023).

[45] M. Leijnse and K. Flensberg, Quantum information transfer between topological and spin qubit systems, Phys. Rev. Lett. **107**, 210502 (2011).

[46] L. N. Zheng, H. F. Wang, and X. X. Yi, Planar and tunable quantum state transfer in a splicing Y-junction Su–Schrieffer–Heeger chain, New J. Phys. **25**, 113003 (2023).

[47] Y. He and C. C. Chien, Non-Hermitian generalizations of extended Su–Schrieffer–Heeger models, J. Phys.: Condens. Matter **33**, 085501 (2021).

[48] C. Wang, L. Li, J. Gong, and Y.-x. Liu, Arbitrary entangled state transfer via a topological qubit chain, Phys. Rev. A **106**, 052411 (2022).

[49] P. Serra, A. Ferrón, and O. Osenda, The scaling law of the arrival time of spin systems that present pretty good transmission, J. Phys. A: Math. Theor. **57**, 015304 (2024).

[50] Z. W. Guo, J. Jiang, H. T. Jiang, J. Ren, and H. Chen, Observation of topological bound states in a double Su-Schrieffer-Heeger chain composed of split ring resonators, Phys. Rev. Res. **3**, 013122 (2021).

[51] A. Youssefi, S. Kono, A. Bancora, M. Chegnizadeh, J. Pan, T. Vovk, and T. J. Kippenberg, Topological lattices realized in superconducting circuit optomechanics, Nature (London) **612**, 666 (2022).

[52] J. X. Han, J. L. Wu, Y. Wang, Y. Xia, Y. Y. Jiang, and J. Song, Large-scale Greenberger-Horne-Zeilinger states through a topologically protected zero-energy mode in a superconducting qutrit-resonator chain, Phys. Rev. A **103**, 032402 (2021).

[53] R. S. Savelev and M. A. Gorlach, Topological states in arrays of optical waveguides engineered via mode interference, Phys. Rev. B **102**, 161112(R) (2020).

[54] C. Vega, M. Bello, D. Porras, and A. González-Tudela, Qubit-photon bound states in topological waveguides with long-range hoppings, Phys. Rev. A **104**, 053522 (2021).

[55] E. Slootman, W. Cherifi, L. Eek, R. Arouca, E. J. Bergholtz, M. Bourennane, and C. M. Smith, Breaking and resurgence of symmetry in the non-Hermitian Su-Schrieffer-Heeger model in photonic waveguides, Phys. Rev. Res. **6**, 023140 (2024).

[56] D. Z. Xie, W. Gou, T. Xiao, B. Gadway, and B. Yan, Topological characterizations of an extended Su–Schrieffer–Heeger model, npj Quantum Inf. **5**, 55 (2019).

[57] N. Goldman, J. C. Budich, and P. Zoller, Topological quantum matter with ultracold gases in optical lattices, Nat. Phys. **12**, 639 (2016).

[58] M. Lohse, C. Schweizer, O. Zilberberg, M. Aidelsburger, and I. Bloch, A Thouless quantum pump with ultracold bosonic atoms in an optical superlattice, Nat. Phys. **12**, 350 (2016).